

Evolution of Shapes of the Subsequence Cavities from the Impact of a Free-Falling Drop

Yu. D. Chashechkin^{a,*} and A. Yu. Ilinykh^{a,**}

Presented by Academician V.F. Zhuravlev September 23, 2021

Received September 26, 2021; revised September 26, 2021; accepted October 20, 2021

Abstract—The evolution of the shape of a sequence of cavities accompanying the coalescence a freely falling drop with a liquid at rest is traced by the method of high-speed video recording. The flow is visualized by the dark field method in the side view (the line of sight lies on the free surface), as well as in the LED-based back-light. In the first case, LED sources were installed on top and on the side of the transparent cuvette; in the second case, a spotlight located behind the cuvette was added to the LED sources. For the first time, the high-resolution experimental technique allows registering the bottom oscillations of the secondary cavities and visualizing the groups of gas bubbles, including frozen-in ones, which reproduce the initial shape of the rapidly filling second cavity, which is formed during splash coalescence. The next shallow cavity is formed after the splash top is submerged. The last cavity is formed by a returning drop previously ejected from the top of the splash. An increase in the rate of the collapsing cavity depth is associated with the conversion of the available potential surface energy (APSE) with a decrease in the area of the free surface of the fluid.

Keywords: drop, cavity, splash, waves, gas bubbles

DOI: 10.1134/S1028335821120028

The observed growth of interest in studying flows generated in liquid at rest by a free falling drop, which were systematically investigated as early as at the end of 19th century [1], is due to the combined action of several factors. The graceful shapes of fast changing structural flow components, the drop itself, the cavity, and the crown are actively reproduced in paintings, sculptures, and jewelry. It is of scientific interest to study the mechanisms of the substance, momentum, and energy transport through the liquid–gas contact surface. Applied interest is caused by expanding areas of application of dropping technologies in chemical, petrochemical, biochemical, pharmaceutical, and other industrial fields.

Dropping flows play an important role in the dynamics of the environment: atmosphere and hydrosphere. In the course of coalescence of a single drop and a liquid, small droplets are ejected from the tips of fine jets at the boundary of the primary contact and at the crown edge and larger drops are ejected from the top of the splash (cumulative jet) and from the subsequent thinner central jet, the streamer. Recent experi-

ments have shown that small droplets are ejected cyclically [2]. Studies of the geometry of the cavity, the splash, and the drops ejected from the top of the latter were performed in [3, 4].

Mineral and organic substances end up in the atmosphere. Mineral remainders of dried drops are carried away to the low-density atmosphere, where they become condensation centers playing an important role in generation of clouds and weather formation [5]. Microorganisms and viruses transferred by wind over great distances can be disease agents of plants and animals and promote propagation of dangerous infections [6].

Along with ejection of sputter into the atmosphere, falling drops activate the transport of the gases both dissolved in them and formed by submerged bubbles into the liquid. Experiments with illumination in the visible and X-ray ranges demonstrated that, in the course of coalescence, a drop is separated from the target liquid by a fine disk-shaped gas layer [7]. Depending on the experimental conditions, the air disk may contract into a single bubble or several gas bubbles or transform in a toroidal cavity [8].

New groups of bubbles fall into liquid at different stages of evolution of the flow. Small bubbles are generated at the contact between the emerging thin water disk (ejecta [9]) and the surface of the target liquid. Large bubbles appear during detachment of a part of

^a *Ishlinsky Institute for Problems in Mechanics, Russian Academy of Sciences, Moscow, Russia*

**e-mail: chakin@ipmnet.ru*

***e-mail: ilinykh@ipmnet.ru*

cavity [10], and the largest ones arise when the edges of the crown and cavity come together [11]. The dynamics of bubble formation becomes more complicated at small drop fall velocities in the range of changing flow patterns, including the modes of coalescence, hanging, reflection, and ejection of a drop part [12]. In the course of subsequent evolution of the flow, several groups of bubbles are observed in the target liquid under submergence of the splash, streamer, and drops that emerged from their tops [13].

The variations in the flow structure are accompanied by the generation of waves, both gravitational-capillary and acoustic ones [14]. Intense ring capillary waves envelope the region of drop spreading [15]. Short waves are observed on the surface of the crown and cavity [16]. Thin jets are generated in the neighborhood of the primary contact region of coalescing liquids, where the free surface is rapidly destroyed and the available potential surface energy (APSE) is transformed into another forms. Separate fast droplets (sputter) emerging from the tops of fine jets form groups of short waves on the surface of the submerging drop [17].

With the development of the microphone and hydrophone at the beginning of the last century, there began the scientific study of the acoustics of drops falling into water that generate the noise of rain [18]. The complete signal includes a high-frequency wave packet of the primary contact of the drop and a group of delayed comparatively low-frequency waves [19]. Combined registration of the flow pattern and acoustic signals allowed determining the oscillating bubbles as one of the main sources of sound [19]. Bubble oscillations are caused by rapid deformation at intake of the cusped remainder of the destroyed fine bridge connecting the detached bubble with the gas medium [20].

Initially, sound signals were identified as tonal, the frequency of which agrees with the estimates of radiation of the oscillating spherical bubble [19]. In the experiments, the range of parameters of the existing sounding bubbles was determined and the map of modes on the plane spanned by the drop diameter and the contact velocity was drawn [19]. Subsequent application of more accurate equipment and data processing programs demonstrated that the spectrum of the signal is multifrequency and the dominating frequency shifts in the course of radiation and varies under the preserved experimental conditions [21]. The time range between acoustic packets also varies in wide ranges, from 0.06 to 0.18 s.

Systematic studies showed that the parameter range of the generation of large gas bubbles is particularly broad and does not form a closed region of existence on the map of modes [19, 22]. Sound radiation is greatly affected by the shapes of the perturbed surface, of the splash, and of the drop ejected after it. In several experiments bubble generation is related by covering of the narrow cavity generated upon submer-

gence of the splash by a previously emerging drop following it [14, 23].

Since the experimental technique with an LED-based backlight [23] does not allow visualizing the evolution of the fine structure of the flow and determining how the hydrodynamic and acoustic phenomena interrelate, the flow pattern under submergence of the splash needs additional investigation. To obtain a more complete answer to the question in the title of paper [22] "Do we understand bubble formation by a single drop impacting upon a liquid surface?," the cavities were first visualized following the spreading of a freely falling drop and the subsequent splash (cumulative jet) in the liquid at rest.

The methodological basis of the work is the system of fundamental equations of fluid mechanics, which is not given here for brevity's sake. It includes the transport equation of the total energy, which allows taking into account the rapid transformation of the APSE into other forms: perturbation of temperature, pressure, and velocity of the fine flow under coalescence of liquids, and a comparatively slow recovery of the APSE under formation of the new free surface.

The media are characterized by the following physical parameters: the densities of air ρ_a and water ρ_d (below, $\rho_{a,d}$), the kinematic $\nu_{a,d}$ and dynamic $\mu_{a,d}$ viscosities of media, the total σ_d^a and density-normed

$\gamma = \frac{\sigma_d^a}{\rho_d} \text{ cm}^3/\text{s}^2$ surface tension coefficients, the free fall acceleration g , the diameter D , the surface area S_d , the volume V_d , the mass M , and the velocity U at the instant of contact. The set of problem parameters also includes the APSE $E_\sigma = \sigma S_d$ concentrated in the spherical layer with a thickness on the order of the molecular cluster, $\delta_\sigma \sim 10^{-6} \text{ cm}$, and the kinetic energy $E_k = \frac{MU^2}{2}$.

In the experiments, a water drop with a diameter $D = 0.42 \text{ cm}$ freely falls from the height $H = 53 \text{ cm}$ and comes into contact with the target liquid with a velocity $U = 3.1 \text{ m/s}$ (the value was determined by the videos). The surface energy of the drop was $E_\sigma = 4 \mu\text{J}$

(it is density is $W_\sigma = \frac{E_\sigma}{V_\sigma} = 2.9 \mu\text{J}/\text{m}^3$), and the kinetic energy was $E_k = 200 \mu\text{J}$. The ratio of the energy components was $E_R = \frac{E_k}{E_\sigma} = 48$, a the density $W_R = \frac{E_k V_\sigma}{E_\sigma V_D} = 1.7 \times 10^{-3}$. The time of transfer of the kinetic energy

counted to $\tau = \frac{D}{U} \sim 3 \text{ ms}$, and the duration of release of the APSE at the primary contact was on the order of $\tau \sim \frac{\delta_\sigma}{U} \sim 10 \text{ ns}$.

The dimensionless conditions of experiments are characterized by the Reynolds number $Re = \frac{UD}{\nu} = 13\,300$, the Froude number $Fr = \frac{U^2}{gD} = 228$, the Bond number $Bo = \frac{gD^2}{\gamma} = 2.5$, the Ohnesorge number $Oh = \frac{\nu}{\sqrt{\gamma D}} = 0.0018$, and the Weber number $We = \frac{U^2 D}{\gamma} = 570$.

The experiments were conducted with the stand for registration of fine-structure rapidly occurring processes, a part of the Unique Research Installations of the Hydrophysical Complex at the Ishlinskii Institute for Problems in Mechanics, Russian Academy of Sciences [24]. A glass basin with dimensions $10 \times 10 \times 7$ cm was partially filled with a degassed pot of water. The flow pattern was illuminated by the spotlights ReyLab Xenos RH-1000, spotlights Optronis MultiLED, and light conduits with LED sources. The flow field was registered by an Optronis CR 300 \times 2 video camera with a framing rate of 4000 frames/s.

Special attention was paid to visualization of the fine structure of three-dimensional flows. We mainly used two techniques. In the first technique, to obtain hard images of the cavity wall and gas bubbles, the light conduits were placed above the splash region, and the spotlights were placed on the side of the splash. Then, we inverted the images obtained above the dark background. In the second technique, we added a spotlight ReyLab in the position to provide light, when the light from the source was directed in the camera objective through the basin with the target liquid.

The evolution of the flow pattern arising at drop spreading in water is illustrated by a sample of frames of the video given in Fig. 1. Coalescence of a drop opened by contact and destruction of free surfaces of liquids is accompanied by the transfer of momentum, the kinetic energy of the drop, and a rapid release of the APSE at the contact spot of the coalescing liquids [2, 14]. Concurrently, a fine veil, a crown with a dissected edge, thin radial jets at its ledges, and small droplets (sputter) emerging from their tips in a wide range of angles to the horizon from 10° to 40° are generated. The bottom cavity at the initial stage of drop spreading is flat and has small irregularities (Fig. 1, $t = 1.25$ ms).

Below, when the cavity shape becomes closer to the half-spherical shape, the cavity bottom descends with the velocity $U_c = 1.6$ m/s. When the cavity depth reaches the maximum, $h_c = 13.6$ mm, capillary waves with a length in the range of $2 < \lambda_c < 5.6$ mm begin to propagate from the crown edge. The combined action

of the surface tension and gravity causes collapse of the cavity, and the velocity of its flattening bottom gradually increases up to $U_c = 0.68$ m/s.

In this mode of flows, the collapse of the cavity is accompanied by generation of the splash, a jet above the surface of the target liquid. As the gravity potential energy and the APSE increase, the motion of the splash tip decelerates. At $t = 133.75$ ms, a drop with diameter $d_s = 0.7$ cm detaches from the conical splash tip.

The splash tip at drop detachment is covered with short capillary waves with a length of $\lambda_s < 0.6$ mm and rapidly moves downwards with an initial velocity of $v_s \approx 1$ m/s. The displacement is ensured by concordant action of the gravity and surface tension causing flattening of the tip (at $t = 135.5$ ms, the curvature radius is $R_s = 0.65$ mm; at $t = 137$ ms, $R_s = 1.3$ mm; and it reaches $R_s = 2.64$ mm at $t = 143$ ms). The secondary drop can preserve its position for some time and then begin to fall; its lower edge moves with a velocity of $U_d = 0.5$ m/s at $t = 137.5$ ms. After that, the drop shape begins to change and the velocity of the lower edge increases up to $U_d = 0.64$ m/s at $t = 144.25$ ms.

Under the submerging splash, the second cavity of a half-spherical shape begins to generate at $t = 135$ ms, gradually deforms, and acquires a conical shape at $t = 137$ ms. Strong interaction of the flows of the submerging splash and the target liquid is indicated by small-scale irregular displacement of the cavity walls beginning at $t = 143$ ms (an enlarged image is presented in Fig. 2). In the lower part of the cavity with a flattening bottom, there appears a group of capillary waves propagating towards the free surface (light strips dissecting the cavity in Fig. 1 at $t = 143$ ms).

The edge of the cavity bottom submerges with a constant velocity $U_c = 0.92$ m/s until the depth $h_c = 1.83$ mm. The first local maximum with a depth $h_c = 2$ mm is achieved at $t = 138.5$ ms, and the cavity bottom is smoothened. Afterwards, after an insignificant reduction, the cavity depth again grows and reaches $h = 2$ mm at $t = 142.5$ ms (the periodogram of the variation in the cavity depth is given in Fig. 3). Simultaneously with the bottom oscillations, the right side of the cavity is filled with water over the entire depth, which is indicated by the clarification of the image near the lateral wall. The inclined water–air contact boundary in the cavity moves in the horizontal direction with a velocity of $U_b = 6$ m/s, and the flattening bottom moves upwards with a velocity $U_c = 2$ m/s, $t = 143.5$ ms.

After filling the cavity, a family of small gas bubbles remains in the liquid, and this family repeats the cavity shape before the fulfillment (they have been probably located at the cavity wall and frozen-in under rapid fulfillment). The preserved bubble trace becomes blurred by subsequent rapid flows generated due to

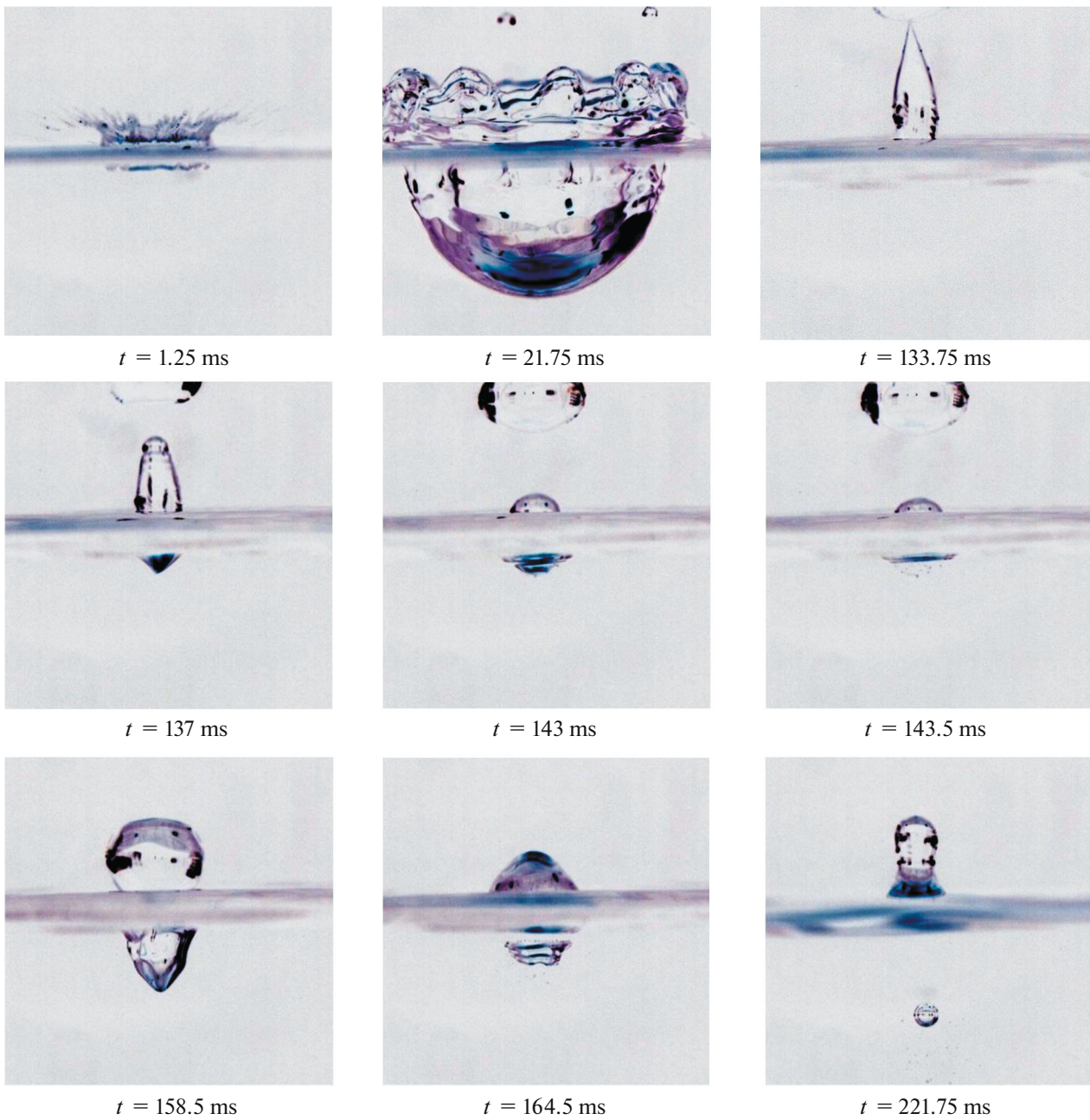


Fig. 1. Evolution of the flow pattern in the vertical plane upon spreading of a free falling water drop in water ($D = 0.42$ cm and $U = 3.1$ m/s); the image is inverted.

transfer of the kinetic energy of the splash and rapid conversion of the APSE upon elimination of the splash free surface and the deformed surface of the liquid.

Herewith, the splash tip continues to submerge with a velocity 0.85 m/s and $t = 144$ ms, and a new cusped cavity with the depth $h_c = 6.3$ mm is formed in the liquid. The complex shape of the gas cavity at $t = 158.5$ ms which has concave segments indicates the

intense flows in the adjacent liquid [14]. Fulfillment of the cavity with the liquid pushing the air begins suddenly. The cavity bottom flattens, and its lower edge moves with a velocity $U_c = 0.5$ m/s. On the lateral surface, we see crests and troughs of capillary waves with the length $\lambda_c = 0.8$ mm.

The velocity of motion of the upper edge of the descending drop counts to $U_d = 0.4$ m/s, $t = 158$ ms, which further increases to $U_d = 0.6$ m/s, $t = 164$ ms,

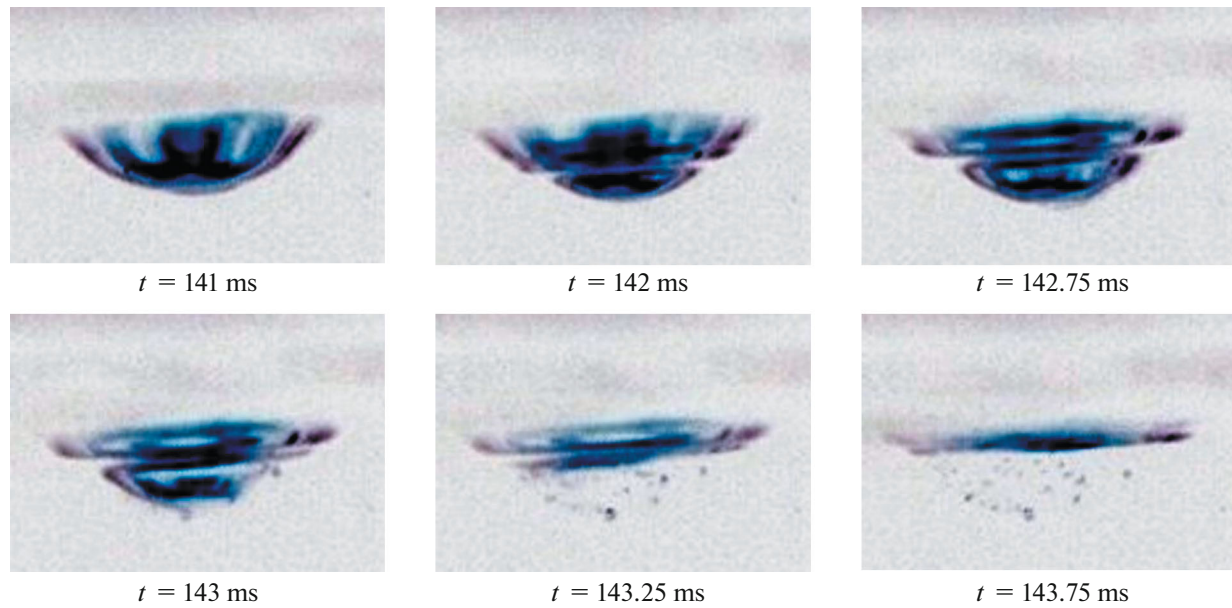


Fig. 2. Cavity collapse at splash submergence and the appearance of a group of frozen-in small bubbles ($D = 0.42$ cm and $U = 3.1$ m/s).

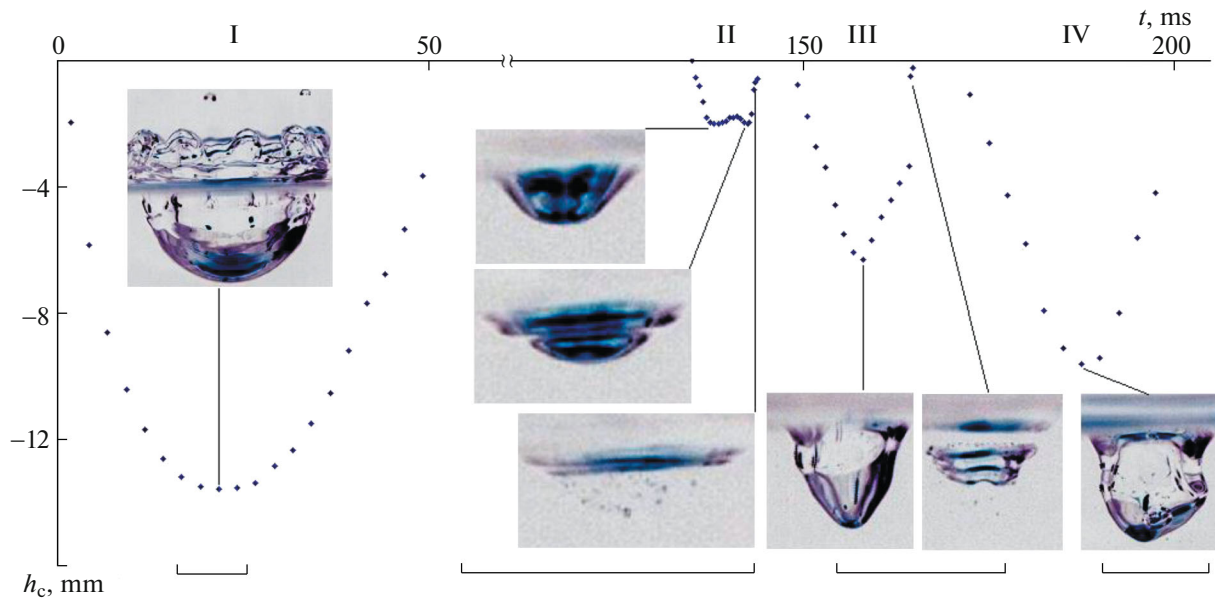


Fig. 3. Variations in the depth and inverted photos of the flow ($D = 0.42$ cm and $U = 3.1$ m/s); cavities: I, primary cavity; II, cavity under the submerged splash; III, cavity following the spreading of a splash top; IV, cavity of a returned secondary drop emerging from the splash top. The lengths of markers are 1 cm.

and reaches $U_d = 1$ m/s at the end of the coalescence process. An increase in the displacement of the upper edge of the drop reflects the influence of the variation in the surface energy at the contact between the drop and the deformed surface of the target liquid. The shape of the remainder of the drop changes and the drop tip sharpens and becomes conical (Fig. 1, $t = 164.5$ ms). The cavity walls are rapidly distorted by troughs, crests, and short capillary waves.

When the cavity generated after the complete coalescence of the returning drop of the splash contracts, in the center of the perturbation region a jet thinner than the splash, called a streamer [21], is generated, and a gas bubble is pushed into the liquid (Fig. 1, $t = 221.75$ ms).

The evolution of the flow pattern in the lower part of the filling secondary cavity of the submerged splash

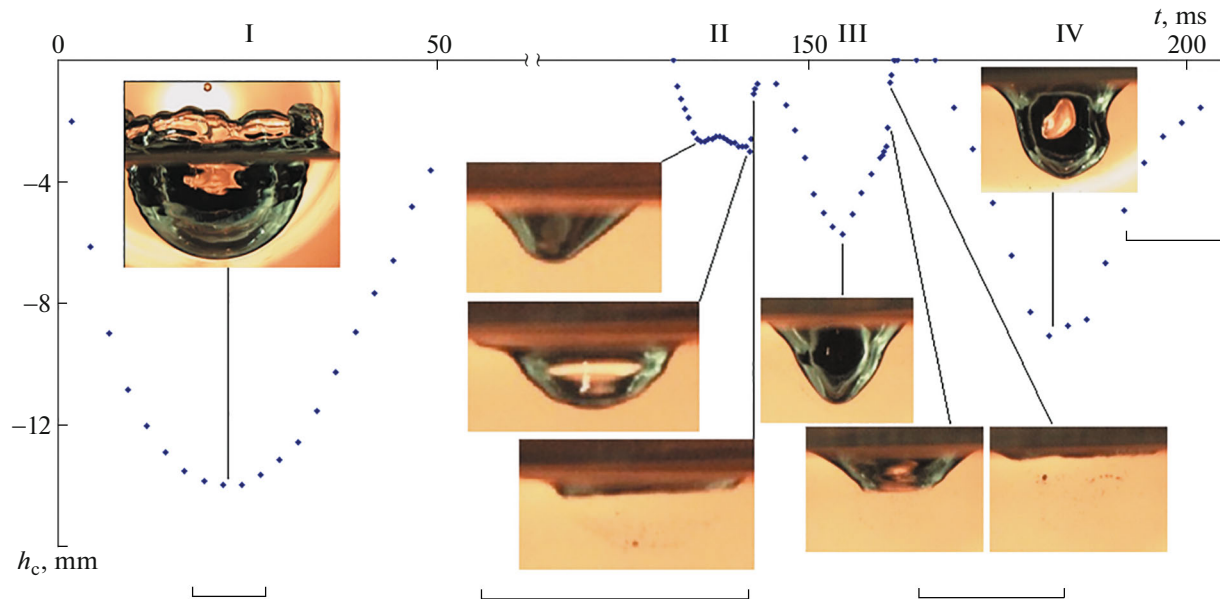


Fig. 4. Variations in the depth and direct photos of the flow pattern of a drop impact ($D = 0.42$ cm and $U = 3.1$ m/s). The lengths of markers are 1 cm.

is traced in Fig. 2. Collapse is preceded by formation of fine perturbation near the bottom of the cavity at $t = 141$ ms. Deformation of the cavity contour is caused by running ring capillary waves visualized by a light strip at $t = 142$ ms moving from the bottom to the free surface (for time $\Delta t = 0.75$ ms the wave shifts over a height of $\Delta z \sim 0.3$ mm).

Filling of the gas cavity upon submergence of a splash occurs both at the bottom and at the lateral wall, which is indicated by the clarification of the image near the lateral wall ($t = 142$ ms). After passage of the interface, a family of gas bubbles is visualized in the bulk of the liquid (dark points on the light background in the right-hand part of the image). The velocity of motion of the inclined boundary (zip fastener by the terminology of [25]) is $U_b = 3.4$ m/s. After $\Delta t = 0.25$ ms, the image of the cavity bottom becomes lighter. In the next frame the entire cavity appears to be completely filled with the liquid. The light strip in the upper dark region is the crest of ring waves. After $\Delta t = 0.5$ ms, the bottom becomes level and the entire cavity presented in Fig. 2, $t = 141$ ms, appears to be filled with liquid containing gas bubbles of different diameters.

Comparison of the flow patterns at $t = 142$ and 143.75 ms shows that bubbles are frozen-in in the liquid and are practically motionless. The boundary of the region with the main mass of bubbles (some of them are outside this region) repeats the cavity shape at $t = 141$ ms.

The secondary drop from the jet tip falls into the perturbed surface of the liquid in which there remain

active flows and waves formed upon submergence of a splash and the cavity remainder. Hence, the drop contact with the smooth surface does not occur at its tip as in the contact of the primary drop, but there is a ring line of contact with the lateral surface of the cavity (Fig. 1, $t = 164.5$ ms). Covering of the cavity remainder leads to capture of air and pushing the gas cavity of irregular shape, which transforms into the oscillating gas bubble. The bubble shape gradually smoothens and becomes spherical (Fig. 1, $t = 221.75$ ms). The further spreading of the splash drop results in formation of the next cavity with a larger maximum depth ($h_c = 9.6$ mm).

In Figs. 3 and 4, we present the periodograms of depth variation and enlarged images of the observed cavities for the two visualization techniques: on the dark background and with activation of the approaching light flux. The insets present the cavities at different stages of evolution, and each group of images is given with its own scale. The main geometric and time parameters of the generation and collapse of cavities are given in Table 1.

The geometry and dynamics of the primary cavity has been reproduced sufficiently accurately in the different experiments, and the duration of its existence was $\Delta t = 49.25$ ms in both experiments. After that, with a delay of $\Delta t = 133.75 \pm 1.5$ ms, related to the motion of the splash and the drop from its tip, the formation of subsequent cavities begins, which is accompanied by the injection of large and small bubbles.

It is characteristic of the second cavity related to the submergence of the splash that there are two local maximums of depth caused by the complicated char-

Table 1

| Cavity no. | 1 | | 2 | | 3 | | 4 | |
|--------------------|-------|-------|-------|--------|-----------|---------|------|----------|
| Experiment no. | I | II | I | II | I | II | I | II |
| Delay, ms | 0 | 0 | 135 | 132.25 | 148 | 144.75 | 171 | 166.75 |
| Lifetime, ms | 49.25 | 49.25 | 9 | 12.5 | 16.5 | 17.25 | 27.5 | 35 |
| Maximum depth, mm | 13.6 | 14 | 2 | 2.9 | 6.3 | 5.7 | 9.6 | 9.1 |
| Growth rate, m/s | 1.6 | 1.65 | 0.8 | 0.95 | 0.7 | 0.73 | 0.64 | 0.63 |
| Collapse rate, m/s | 0.68 | 0.54 | <3.12 | <5.9 | 0.47–11.4 | 0.5–5.9 | 0.69 | 0.1–0.69 |

acter of interaction of the submerged splash with the moving liquid in which fine flows are preserved accompanying the evolution of the primary cavity.

After its collapse, the second cavity growing in the course of splash submergence leaves a cloud of small bubbles reproducing its primary shape. The third cavity is associated with passage of the upper edge of the splash through the free surface. It is distinguished by a cusped shape with sharp wrinkles caused by strong interactions of the submerging liquid with the remaining flows in the liquid. In the evolution of both cavities in the experiments presented, an increase in the depth and subsequent collapse appear practically linearly.

The main part of the process of cavity collapse occurs particularly rapidly, over 0.5–1 ms. Afterwards, the boundary of the cavity remainder moves linearly towards the initial position of the free surface. The fourth cavity arising upon coalescence of the previously ejected drop of the splash with the deformed surface of the liquid in which the cavity remains after partial collapse of the third cavity has the most complicated and irregular shape dissected by capillary waves, individual bulges, and troughs [14].

A smooth increase in the cavity depth when the kinetic energy converges to the potential gravitational energy and APSE differs significantly from the non-uniform rate of decrease in the depth at the end of the collapse process. Here, we observe an additional acceleration of the bottom motion caused by a rapid release of the APSE and its transformation into other shapes. At this stage, there occurs formation of rapidly moving gas cavities radiating sound.

The general pattern of the flows and the dynamics of the variation in the cavity dimensions are stably reproduced in different experiments. The collapse of the second cavity with the formation of a cloud of frozen-in bubbles was observed in all experiments conducted in this flow mode.

ACKNOWLEDGMENTS

This study was conducted on the stands of the Unique Research Installations of the Hydrophysical Complex, Ishlinsky Institute for Problems in Mechanics, Russian Academy of Sciences.

FUNDING

This work was supported by the Russian Science Foundation, project no. 19-19-00598.

REFERENCES

1. A. M. Worthington, *The Splash of the Drop* (E. J. Young, New York, 1895).
2. V. A. Arkhipov and V. F. Trofimov, *Prikl. Mekh. Tekh. Fiz.* **46**, 55 (2005).
3. E. Castillo-Orozco, A. Davanlou, P. K. Choudhury, and R. Kumar, *Phys. Rev. E* **92**, 053022 (2015). <https://doi.org/10.1103/PhysRevE.92.053022>
4. Yu. D. Chashechkin and A. Yu. Ilinykh, *Dokl. Phys.* **65**, 366 (2020). <https://doi.org/10.1134/S1028335820100067>
5. F. Veron, *Ann. Rev. Fluid Mech.* **47**, 507 (2015). <https://doi.org/10.1146/annurev-fluid-010814-014651>
6. B. D. L. Fitt, H. A. McCartney, and P. Walkalate, *Ann. Rev. Phytopath.* **27**, 241 (1989). <https://doi.org/10.1146/annurev.py.27.090189.001325>
7. S. Thoroddsen, T. Etoh, and K. Takehara, *J. Fluid Mech.* **478**, 125 (2003). <https://doi.org/10.1017/S0022112002003427>
8. Z. Jian, M. A. Channa, A. Kherbeche, H. Chizari, S. T. Thoroddsen, and M.-J. Thoraval, *Phys. Rev. Lett.* **124**, 184501 (2020). <https://doi.org/10.1103/PhysRevLett.124.184501>
9. G. Liang, Y. Guo, S. Shen, et al., *Theor. Comput. Fluid Dyn.* **28**, 159 (2014). <https://doi.org/10.1007/s00162-013-0308-z>
10. S. Phillips, A. Agarwal, and P. Jordan, *Sci. Rep.* **8**, 9515 (2018). <https://doi.org/10.1038/s41598-018-27913-0>
11. H. Deka, B. Ray, G. Biswas, A. Dalal, P.-H. Tsai, and A.-B. Wang, *Phys. Fluids* **29**, 09210 (2017). <https://doi.org/10.1063/1.4992124>
12. Yu. D. Chashechkin and A. Yu. Ilinykh, *Fluid Dyn. Mater. Process.* **16**, 801 (2020). <https://doi.org/10.32604/fdmp.2020.09168>
13. H. C. Pumphrey and P. A. Elmore, *J. Fluid Mech.* **220**, 539 (1990). <https://doi.org/10.1017/S0022112090003378>
14. Yu. D. Chashechkin, *Vestn. MGTU Baumana, Ser. Estestv. Nauki*, No. 1 (94), 73 (2021). <https://doi.org/10.18698/1812-3368-2021-1-73-92>

15. Z. Guo Zhen, L. Zhao Hui, and F. de Yong, *Chin. Sci. Bull.* **53**, 1634 (2008).
<https://doi.org/10.1007/s11434-008-0246>
16. Yu. D. Chashechkin and V. E. Prokhorov, *Dokl. Phys.* **58**, 296 (2013).
<https://doi.org/10.1134/S1028335813070021>
17. Yu. D. Chashechkin and A. Yu. Ilinykh, *Dokl. Phys.* **60**, 548 (2015).
<https://doi.org/10.1134/S1028335815120022>
18. I. V. Vovk and V. T. Grinchenko, *Sound, Born of a Stream (Essay on Aerohydrodynamic Acoustics)* (Naukova Dumka, Kiev, 2010) [in Russian].
19. A. Prosperetti and H. N. Oguz, *Ann. Rev. Fluid Mech.* **25**, 577 (1993).
<https://doi.org/10.1146/annurev.fl.25.010193.003045>
20. Yu. D. Chashechkin and V. E. Prokhorov, *Dokl. Phys.* **60**, 355 (2015).
<https://doi.org/10.1134/S1028335815080054>
21. Yu. D. Chashechkin and V. E. Prokhorov, *Acoust. Phys.* **66**, 362 (2020).
<https://doi.org/10.1134/S1063771020040016>
22. A. Wang, C. Kuan, and P. Tsai, *Phys. Fluids* **25**, 101702 (2013).
<https://doi.org/10.1063/1.4822483>
23. G. Gillot, C. Derec, J.-M. Genevieux, L. Simon, and L. Benyahia, *Phys. Fluids* **32**, 062004 (2020).
<https://doi.org/10.1063/5.0010464>
24. Hydrophysical Complex for Modeling Hydrodynamic Processes in the Environment and Their Impact on Underwater Technical Objects, as well as the Propagation of Impurities in the Ocean and Atmosphere.
<http://www.ipmnet.ru/uniquequip/gfk/#equip>.
25. G. Gillot, L. Simon, J.-M. Genevieux, and L. Benyahia, *Phys. Fluids* **33**, 077114 (2021).
<https://doi.org/10.1063/5.0055361>

Translated by E. Oborin